Journal of Biomechanics ▮ (▮▮▮▮) ▮▮▮–▮▮▮

Contents lists available at ScienceDirect

Journal of Biomechanics

journal homepage: www.elsevier.com/locate/jbiomech
www.JBiomech.com

# Circumferential variations of mechanical behavior of the porcine thoracic aorta during the inflation test

Jungsil Kim, Seungik Baek *

*Department of Mechanical Engineering, Michigan State University, 2457 Engineering Building, East Lansing, MI 48824-1226, USA*

ARTICLE INFO

*Article history:*
Accepted 19 April 2011

*Keywords:*
Vascular stiffness
Heterogeneity
Strain analysis
Stereo vision system

ABSTRACT

We developed an extension-inflation experimental apparatus with a stereo vision system and a stress–strain analysis method to determine the regional mechanical properties of a blood vessel. Seven proximal descending thoracic aortas were investigated during the inflation test at a fixed longitudinal stretch ratio of 1.35 over a transmural pressure range from 1.33 to 21.33 kPa. Four circumferential regions of each aorta were designated as the anterior (A), left lateral (L), posterior (P), and right lateral (R) regions, and the inflation test was repeated for each region of the aortas. We used continuous functions to approximate the surfaces of the regional aortic wall in the reference configuration and the deformed configuration. Circumferential stretch and stress at the four circumferential regions of the aorta were computed. Circumferential stiffness, defined as the tangent of the stress–stretch curve, and physiological aortic stiffness, named pressure–strain elastic modulus, were also computed for each region. In the low pressure range, the stress increased linearly with increased stretch, but the mechanical response became progressively stiffer in the high-pressure range above a transition point. At a transmural pressure of 12.00 kPa, mean values of stiffness were $416 \pm 104$ kPa (A), $523 \pm 99$ kPa (L), $634 \pm 91$ kPa (P), and $489 \pm 82$ kPa (R). The stiffness of the posterior region was significantly higher than that of the anterior region, but no significant difference was found in pressure–strain elastic modulus.

© 2011 Elsevier Ltd. All rights reserved.

## 1. Introduction

While it is well known that the mechanical properties of healthy blood vessels vary with location and age, their circumferential variations have received little attention. In biomechanical analysis of the aorta, it has been typically assumed that aortic thickness is constant and mechanical properties of the aorta are uniform in the circumferential direction. Recent biomedical imaging studies, however, reported that the circumferential deformation and wall distension of the aorta during the cardiac cycle were non-uniform (Draney et al., 2002, 2004; van Prehn et al., 2009). Few experimental studies have quantified the circumferential variations of the mechanical behavior of the aorta.

A variety of testing methods have been employed to characterize the mechanical properties of vascular tissue, including uniaxial and planar biaxial tests (Gundiah et al., 2007; Lally et al., 2004; Okamoto et al., 2002; Sokolis, 2007; Tremblay et al., 2010; Vande Geest et al., 2006; Zhou and Fung, 1997), ring tests (Guo and Kassab, 2004; Huang et al., 2006; Lillie and Gosline, 2007), and inflation tests (Blondel et al., 2001; Humphrey et al., 1993; Langewouters et al., 1984; Schulze-Bauer et al., 2002). It appears that the inflation test is the preferred test for estimating *in vivo* stress, because it closely reflects the motion of the aortic wall during the cardiac cycle. A video-based tracking technique with multiple markers embedded or affixed to the specimen is typically applied in order to enable monitoring of the large deformation of the vascular tissue (Everett et al., 2005; Hsu et al., 1995; Hu et al., 2007; Saravanan et al., 2006; Thubrikar et al., 1990; Zhang et al., 2002). In the traditional *ex vivo* inflation test, a blood vessel is commonly assumed to be a perfect cylindrical tube, and only its outer diameter change was measured during the test (Blondel et al., 2001; Langewouters et al., 1984; Schulze-Bauer et al., 2003; Valdez-Jasso et al., 2009), so that the spatial variation in the local mechanical properties of the vessel was not usually characterized. Recently, advances in three-dimensional (3D) imaging have allowed the use of 3D tracking systems to measure non-uniform deformation during the inflation test. In particular, Genovese (2009) introduced a new optical system with a concave conical mirror, which provides the full-field measurement of 3D deformation of an artery, and Avril et al. (2010) developed an inverse method to derive the material parameters based on the full-field experimental data. However, there is still a need for developing more analysis methods to utilize 3D spatial information in order

* Corresponding author. Tel.: +1 517 432 3161; fax: +1 517 353 1750.
*E-mail address:* sbaek@egr.msu.edu (S. Baek).

0021-9290/$ - see front matter © 2011 Elsevier Ltd. All rights reserved.
doi:10.1016/j.jbiomech.2011.04.022

to characterize the heterogeneity in the mechanical properties of a blood vessel.

In the present study, we developed an extension-inflation experimental apparatus with a stereo vision system and a new stress–strain analysis method, and used them to investigate the circumferential variations in mechanical properties of the porcine thoracic aorta.

## 2. Methods

### 2.1. Experimental system

A computer-controlled system (Fig. 1) was developed to measure the biaxial deformation of a blood vessel during the inflation test. It consists of three main parts: motion, data acquisition, and vision systems.

A polycarbonate test chamber was placed on the lower crosshead in the center of the test device. Two moving crossheads were driven by a stepper motor in opposite directions, while the center of the device remained fixed. The specimen was connected to a syringe pump (KDS 210, KD Scientific, MA, USA) by a tube. Continuous bidirectional infusion-withdrawal motion of the syringe pump cyclically inflated and deflated the specimen.

A 34.47 kPa (5 psi) gauge pressure transducer (FPG2AT, Honeywell-Sensotec, OH, USA) was affixed to the tube connected to the specimen. The transmural pressure was defined as the difference in pressure between the inside and outside of the specimen in the test chamber. The axial load applied to the specimen was measured using a 4.54 kg (10 lb) load cell (Model 34, Tension/Compression, Honeywell-Sensotec, OH, USA) attached to the upper connector of the specimen, although the data on axial load were not used in this paper. The measurements were collected in a computer by a data acquisition board at a 100 Hz sampling rate.

The stereo vision system, consisting of two CCD monochrome cameras (KPM2A, 768H × 494V, Hitachi, Japan) with fixed focal length lenses (HF25HA-1B, Fujinon, Japan), allowed 3D marker tracking during the inflation test. Two cameras were placed at different positions but at the same height, focusing on the central region of the device where the specimen was mounted. The distance from the cameras to the specimen was approximately 30 cm and the included angle between the two cameras and the specimen was approximately 30°. The frame grabber obtained images of the specimen using the two cameras alternately at five frames per 2 s.

### 2.2. Specimen preparation

Aortas from seven approximately six-month-old pigs were obtained from a local vendor and stored at 5 °C until testing within 24 h after death. The peripheral, loose connective tissues were carefully removed from the adventitia, while aortic branches were kept intact (Fig. 2(a)). The straight proximal descending thoracic aorta, approximately 15 cm long, was isolated. All aortic branches were ligated with nylon thread, and the both ends of the isolated aorta were cannulated to connectors with care to ensure the aorta was not bent or twisted. Near the first to third intercostal arteries, 550 μm-diameter black spheres were attached to the aortic wall along its circumference, using a pulled-glass micropipette with a minimal amount of glue, and avoiding the regions of aortic branches (Fig. 2(b)). Additional microspheres were attached to the proximal and distal regions of the specimen to obtain reference measurements of longitudinal stretch. The specimens were mounted vertically in the test chamber and the inside of the specimen and the test chamber were filled with 0.9% NaCl solution.

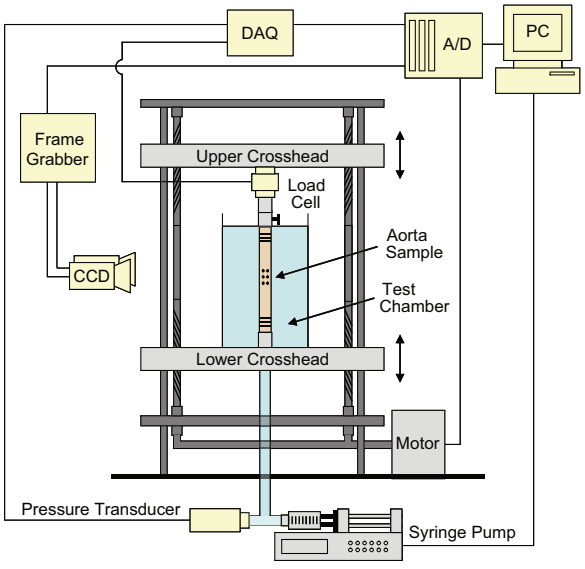


**Fig. 1.** Schematic diagram of the experimental set-up for the extension-inflation test.

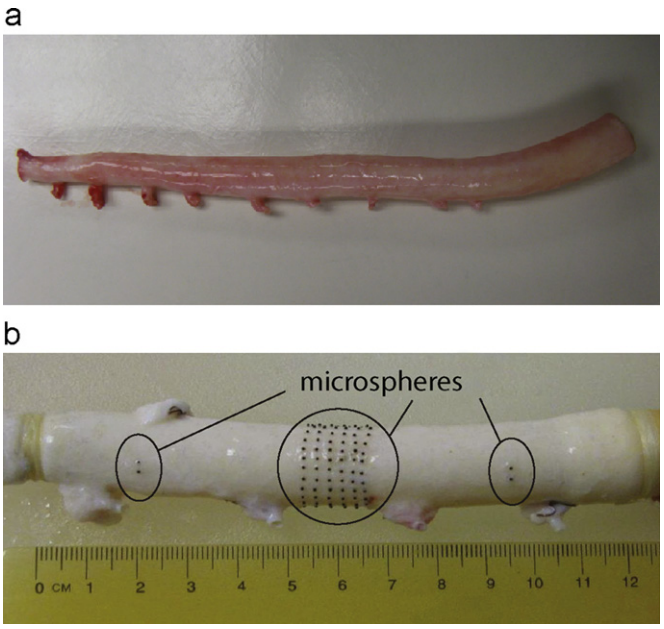


**Fig. 2.** A porcine thoracic aorta after removing surrounding tissues (a) and a cannulated aorta specimen with microspheres affixed on the aortic wall (b).

### 2.3. Test protocol

The reference length at the load-free state, wherein the blood vessel at zero longitudinal force and zero transmural pressure, was recorded, while the force exerted by the vessel weight was ignored. The specimen was preconditioned longitudinally and circumferentially to obtain repeatable mechanical responses and to reduce possible stress induced during the preparation. The specimen was then extended at a stretch ratio of 1.35 with respect to the reference length. The aorta has a pre-stretch in the longitudinal direction at the *in vivo* state, and its *in situ* stretch ratio was estimated between 1.2 and 1.45 (Han and Fung, 1995). Next, the inflation test at a fixed longitudinal stretch ratio was performed by pressurizing and depressurizing the specimen five times at approximately 1/110 Hz frequency over a wide transmural pressure range from 1.33 to 21.33 kPa (10–160 mmHg) at room temperature. Digital images of the specimen were recorded simultaneously with pressure and axial load measurements.

In the present study, we examined mechanical behaviors of the aorta at four circumferential regions. A small region of aortic wall between two consecutive intercostal arteries was defined as the posterior region (P), its opposite across the lumen was defined as the anterior region (A), and the two side regions were determined as the left lateral region (L) and right lateral region (R). The inflation tests were repeated at these four regions after 90° rotations of the specimen from one region to another. Great care was taken that no twisting of the specimen occurred during rotation.

After the inflation test, a cross-sectional cut of the specimen was made at the mid-portion, where the markers were affixed. The wall thickness measurements per specimen were repeated three times at every 45° along the circumference using a vernier caliper.

### 2.4. Camera matrix and 3D image reconstruction

Two CCD cameras obtained serial digital images of the specimen during the test. The region where markers were affixed to the specimen was selected from the image. The centers of markers were extracted in pixels and tracked. A projective camera model, which mapped 3D world points $(X^w, Y^w, Z^w)$ to 2D image points $(x^p, y^p)$ using homogeneous coordinates, was employed. This mapping can

Please cite this article as: Kim, J., Baek, S., Circumferential variations of mechanical behavior of the porcine thoracic aorta during the inflation test. Journal of Biomechanics (2011), doi:10.1016/j.jbiomech.2011.04.022

be written as

$$\begin{Bmatrix} sx^p \\ sy^p \\ s \end{Bmatrix} = \begin{bmatrix} M_{11} & M_{12} & M_{13} & M_{14} \\ M_{21} & M_{22} & M_{23} & M_{24} \\ M_{31} & M_{32} & M_{33} & 1 \end{bmatrix} \begin{Bmatrix} X^w \\ Y^w \\ Z^w \\ 1 \end{Bmatrix}, \quad (1)$$

where $s$ is a scale factor (Shapiro and Stockman, 2001). The $3\times4$ camera matrix $\mathbf{M}$ in Eq. (1), which describes how a point in the world projects onto an image in pixels, was determined by 3D world points on a calibration jig and their corresponding 2D images using the pseudoinverse (least squares) method. Once the matrices of both cameras were determined, the 3D positions of markers were obtained by linear mapping equations derived from Eq. (1) for each cameras using pairs of 2D stereo images taken by both cameras.

## 3. Stress–strain analysis

The surface of each of the four circumferential regions in the reference and deformed configurations was approximated by continuous functions. The approximation and parameter estimation using stereo images are explained in the Appendix A. Here, $\mathbf{X}$ and $\mathbf{x}$ denote the 3D positions of markers in the reference and deformed configurations, respectively.

### 3.1. Deformation gradient, thickness, and curvature

The covariant base vectors $\mathbf{G}_i$ and $\mathbf{g}_i$ of the surface in the reference and deformed configurations, respectively, are defined as

$$\mathbf{G}_i = \frac{\partial \mathbf{X}}{\partial \Sigma_i}, \quad \mathbf{g}_i = \frac{\partial \mathbf{x}}{\partial \Sigma_i}, \quad (2)$$

where the two convected variables are $\Sigma_1 = \overline{\Theta}$ and $\Sigma_2 = \overline{S}$. The contravariant base vectors $\mathbf{G}^j$ in the reference configuration are determined to satisfy the relation

$$\mathbf{G}_i \cdot \mathbf{G}^j = \delta_i^j, \quad (3)$$

where $\delta_i^j = 1$ if $i=j$, and $\delta_i^j = 0$ if $i \neq j$ for $i, j = 1, 2$.

In a convected curvilinear coordinate system, the 2D deformation gradient $\mathbf{F}$ of the surface is given by

$$\mathbf{F} = \mathbf{g}_i \otimes \mathbf{G}^i, \quad (4)$$

where $\otimes$ denotes the tensor product. Since the covariant and contravariant base vectors are generally not orthonormal, local orthonormal base vectors $\hat{E}_i$ in the reference configuration and $\hat{e}_i$ in the current configuration are determined at each point by

$$\hat{\boldsymbol{E}}_1 = \frac{\mathbf{G}_1}{|\,\mathbf{G}_1\,|}, \quad \hat{\boldsymbol{E}}_2 = \frac{\mathbf{G}_2 - (\mathbf{G}_2 \cdot \hat{\boldsymbol{E}}_1)\hat{\boldsymbol{E}}_1}{|\,\mathbf{G}_2 - (\mathbf{G}_2 \cdot \hat{\boldsymbol{E}}_1)\hat{\boldsymbol{E}}_1\,|}, \quad (5)$$

$$\hat{\boldsymbol{e}}_1 = \frac{\mathbf{g}_1}{|\,\mathbf{g}_1\,|}, \quad \hat{\boldsymbol{e}}_2 = \frac{\mathbf{g}_2 - (\mathbf{g}_2 \cdot \hat{\boldsymbol{e}}_1)\hat{\boldsymbol{e}}_1}{|\,\mathbf{g}_2 - (\mathbf{g}_2 \cdot \hat{\boldsymbol{e}}_1)\hat{\boldsymbol{e}}_1\,|}, \quad (6)$$

where the subscripts 1 and 2 represent the circumferential and longitudinal directions, respectively. Finally, the 2D deformation gradient $\mathbf{F}$ with respect to the local orthonormal base vectors can be written as $F_{pq} = \hat{\mathbf{e}}_p \cdot \mathbf{F}\hat{\mathbf{E}}_q$.

In the load-free state, the aortic wall thickness $H_0$ at a given position along the circumference is approximated by a curve fit to the measurements of aortic wall thickness, using Fourier series

$$H_0(\theta) = a_0 + a_1\cos(\theta) + a_2\sin(\theta) + a_3\cos(2\theta) + a_4\sin(2\theta). \quad (7)$$

The deformed wall thickness $h$ during the inflation test is calculated by using the incompressibility assumption ($(h/H_0)$ det $\mathbf{F}=1$) (Carew et al., 1968), therefore

$$h = \frac{H_0}{F_{11}F_{22} - F_{12}F_{21}}. \quad (8)$$

The principal curvature of the aortic wall is obtained by the first and second fundamental forms of a surface in differential geometry. The normal curvatures $\kappa_n$ of a surface are (Struik, 1988)

$$\kappa_n = \frac{L\,d\overline{\Theta}^2 + 2M\,d\overline{\Theta}\,d\overline{S} + N\,d\overline{S}^2}{E\,d\overline{\Theta}^2 + 2F\,d\overline{\Theta}\,d\overline{S} + G\,d\overline{S}^2}, \quad (9)$$

where

$$E = \mathbf{g}_1 \cdot \mathbf{g}_1, \quad F = \mathbf{g}_1 \cdot \mathbf{g}_2, \; G = \mathbf{g}_2 \cdot \mathbf{g}_2, \quad (10)$$

$$L = \mathbf{g}_{1,1} \cdot \hat{N}, \quad M = \mathbf{g}_{1,2} \cdot \hat{N}, \; N = \mathbf{g}_{2,2} \cdot \hat{N}. \quad (11)$$

Here $\mathbf{g}_{i,j}$ denotes $\partial \mathbf{g}_i / \partial \Sigma_j$ and the unit surface normal vector $\hat{N}$ is given by

$$\hat{N} = \frac{\mathbf{g}_1 \times \mathbf{g}_2}{|\mathbf{g}_1 \times \mathbf{g}_2|}. \quad (12)$$

The two extreme values of $\kappa_n$ in Eq. (9) are the two principal curvatures $\kappa_1$ and $\kappa_2$. The outer radii of curvatures of the aortic wall are calculated by $r_i = 1/\kappa_i$ for $i=1, 2$.

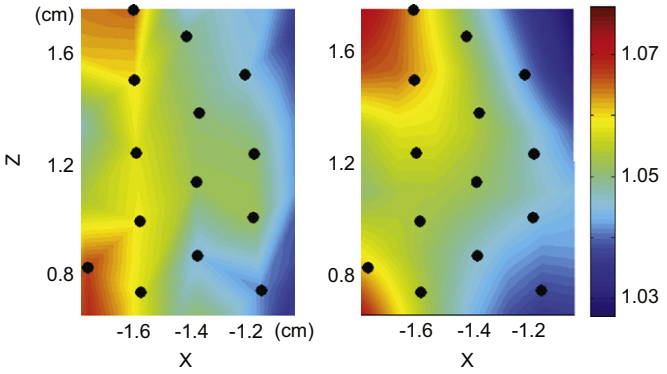


**Fig. 3.** Distribution of circumferential stretches obtained by two methods: (a) a linear approximation with triangular elements and (b) an approximation based on continuous function in the present study. Black dots represent markers in the deformed configuration.

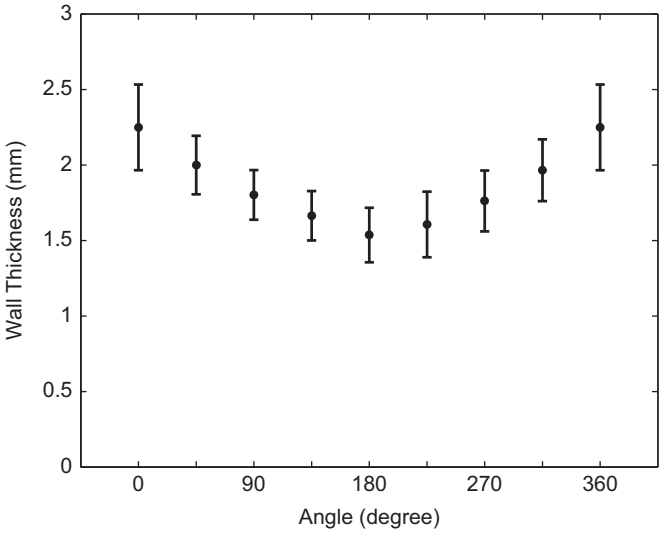


**Fig. 4.** The mean and standard deviation of the aortic wall thickness along the circumference. 0° and 360°: the anterior region, 90°: left lateral region, 180°: posterior region, and 270°: right lateral region.

Please cite this article as: Kim, J., Baek, S., Circumferential variations of mechanical behavior of the porcine thoracic aorta during the inflation test. Journal of Biomechanics (2011), doi:10.1016/j.jbiomech.2011.04.022

### 3.2. Stretch, stress, and stiffness

The circumferential stretch $\lambda$ is calculated at each point by

$$\lambda = \sqrt{\hat{\boldsymbol{E}}_1 \cdot (\mathbf{F}^T\mathbf{F})\hat{\boldsymbol{E}}_1}. \tag{13}$$

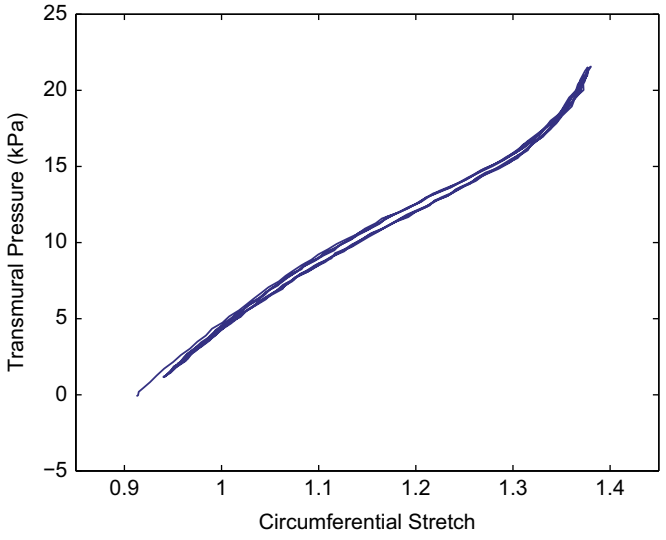


**Fig. 5.** A representative example of the five cyclic loading and unloading curves on a region of an aorta after preconditioning.

Since the mean radius of the curvature in the longitudinal direction is much larger than that in the circumferential direction ($r_2 \gg r_1$), the circumferential Cauchy stress $\sigma$ is estimated by

$$\sigma = \frac{P(r_1 - h)}{h}. \tag{14}$$

The circumferential stiffness $k(P_i)$, which is defined as the tangent of the mean stress–stretch curve, is obtained at a transmural pressure of $P_i$ by

$$k(P_i) = \left.\frac{\partial\sigma}{\partial\lambda}\right|_{\lambda(P_i)} = \frac{\sigma(\lambda+\Delta\lambda) - \sigma(\lambda-\Delta\lambda)}{2\Delta\lambda}. \tag{15}$$

To estimate the structural stiffness during the cardiac cycle, the pressure–strain elastic modulus $E_p$ (Feigl et al., 1963; Peterson et al., 1960) is calculated by

$$E_p = \frac{P_{sys} - P_{dia}}{(\lambda_{sys} - \lambda_{dia})/\lambda_{dia}}, \tag{16}$$

where subscripts *sys* and *dia* denote the systolic and diastolic condition, respectively. We assumed $P_{sys} = 15.20$ kPa (114 mmHg) and $P_{dia} = 10.13$ kPa (76 mmHg).

### 3.3. Statistical analysis

Stiffness for each circumferential region of each specimen was used for statistical analysis. The significance of the difference among the four circumferential regions and each pair of regions was evaluated by using one-way repeated measures ANOVA with

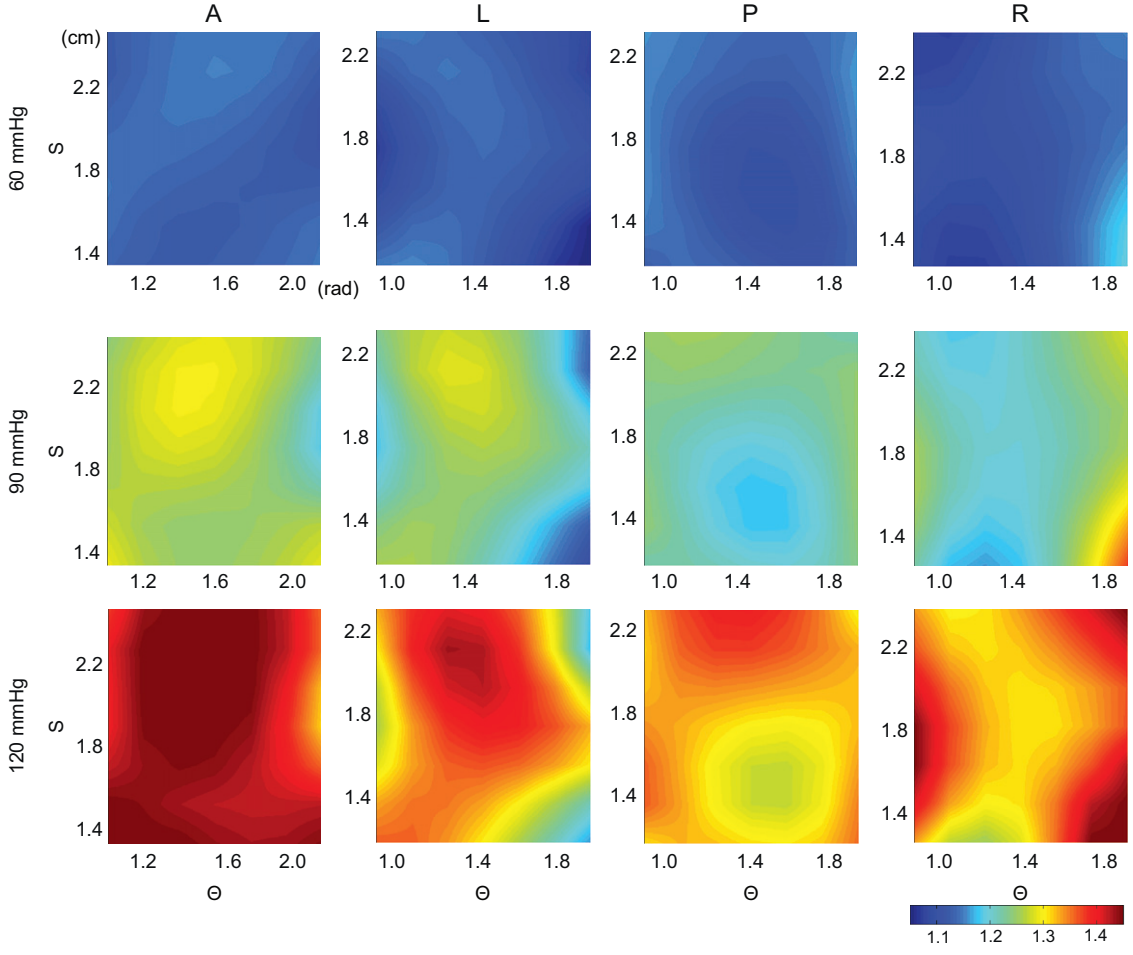


**Fig. 6.** Distributions of the circumferential stretches for four circumferential regions of a sample at transmural pressures of 8.00 kPa (60 mmHg), 12.00 kPa (90 mmHg), and 16.00 kPa (120 mmHg), respectively, and a longitudinal stretch ratio ($\Lambda_Z$) of 1.35. A: anterior region, L: left lateral region, P: posterior region, and R: right lateral region.

Please cite this article as: Kim, J., Baek, S., Circumferential variations of mechanical behavior of the porcine thoracic aorta during the inflation test. Journal of Biomechanics (2011), doi:10.1016/j.jbiomech.2011.04.022

post-hoc tests based on Sidak adjustment. The difference was considered significant when $p < 0.05$.

## 4. Results

### 4.1. Validation of the method

In our pilot study, the inflation test of the same region of the aorta was repeated under the same experimental conditions after rotating the specimen in order to ensure the reproducibility of results. There was little difference between the two stress–stretch responses before and after rotation.

A flexible silicone tube was used to compare the circumferential stretch distributions obtained by two approximations: one was based on the continuous functions explained in the previous section, and the other was based on a linear polynomial approximation with triangular elements, which is a typical method used in finite element analysis and previous experimental studies (Hu et al., 2007; Saravanan et al., 2006). Although the stretch distributions appeared similar, the stretch distribution obtained by the continuous function approximation showed smoother and slightly higher variation than that obtained by the linear approximation (Fig. 3). In addition to the circumferential stretch, the outer radii of the silicone tube obtained by the continuous function approximation and by the least squares method, assuming the tube to be an ideal cylinder with a constant radius, were compared. The radius difference between the two methods was less than 2%.

### 4.2. Wall thickness and curvature

Aortic wall thickness changed gradually along the circumference (Fig. 4). In all aorta samples, the anterior region was the thickest ($2.2 \pm 0.3$ mm) and the posterior region was the thinnest ($1.5 \pm 0.2$ mm).

The outer radius of the aorta changed in response to pressure changes. In the load-free state, the radius of curvature of the posterior region was slightly smaller than that of other regions. During inflation, the radii of the four regions became nearly uniform as pressure was increased. At a transmural pressure of 12.00 kPa, the mean and standard deviation of the radius for each region were $10.0 \pm 0.7$ mm (A), $10.1 \pm 0.7$ mm (L), $10.2 \pm 0.7$ mm (P), and $10.1 \pm 0.8$ mm (R).

### 4.3. Mechanical response of the aorta

In a cyclic loading condition, loading and unloading curves exhibited small hysteresis (i.e., pseudo-elastic behavior, Fig. 5). Therefore, the last loading curve was used for stress–strain analysis.

The circumferential stretch (Fig. 6) and the circumferential Cauchy stress were distributed nonuniformly, varied within the local circumferential regions, and changed gradually as the pressure increased. The stretch and stress values averaged within each region were calculated for comparison. Fig. 7(a) displays the stress–stretch responses plotted for the four regions of a specimen. These curves deviated progressively as the pressure increased, and all aorta samples exhibited similar nonlinear behavior. In the low pressure range, the stress–stretch response for each region was nearly linear, but the response became nonlinear in the high-pressure range after the transmural pressure reached a transition point, which ranged from 10.93 to 14.53 kPa (82–109 mmHg). In Fig. 7(b), the circumferential stiffness of the four regions is plotted with respect to the pressure. In the low pressure range, the stiffness was nearly constant and

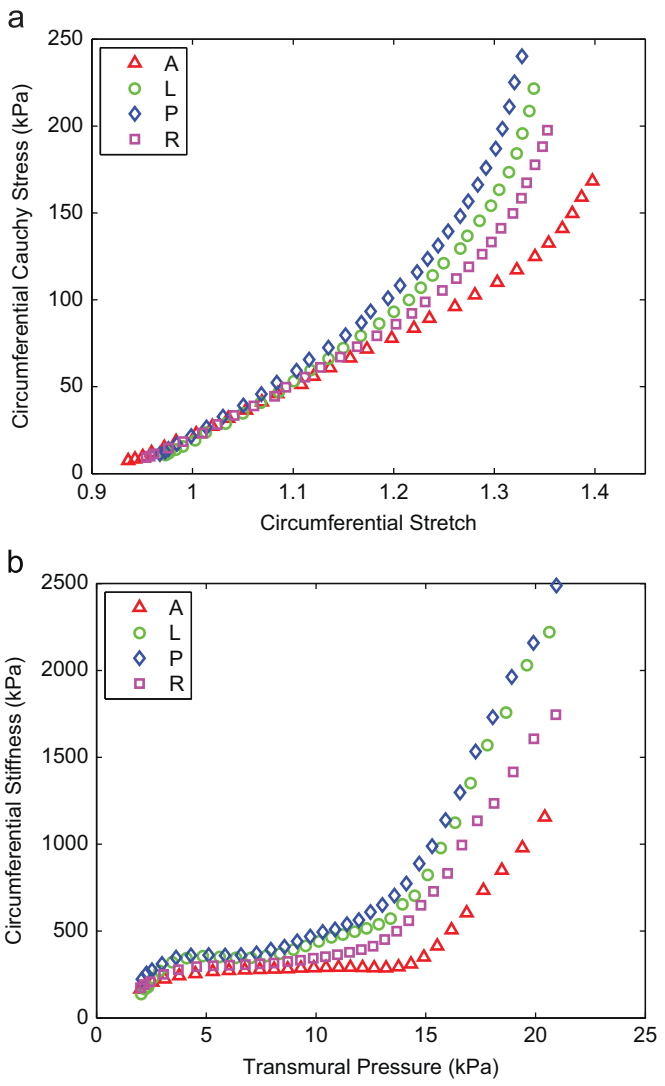


**Fig. 7.** A representative example of (a) the circumferential Cauchy stress and stretch plot and (b) the circumferential stiffness ($k$) and transmural pressure plot, at $\lambda_Z = 1.35$.

corresponded to the linear stress–stretch response, but increased markedly after the transition point.

For each region of each specimen, average stretch and stress values were obtained, and the mean of these values was then obtained over the seven aorta samples. No significant difference in the mean stretches of the four regions (Fig. 8(a)) was found, but there was significant difference in the mean stresses among the four regions above a transmural pressure of 8.00 kPa (60 mmHg). The mean and standard deviation of stress averaged within each region at a transmural pressure of 12.00 kPa (90 mmHg), which is near the transition point, were $82 \pm 16$ kPa (A), $100 \pm 16$ kPa (L), $113 \pm 17$ kPa (P), and $96 \pm 17$ kPa (R) (Fig. 8(b)).

Mean stiffness for each region at transmural pressures of 8.00, 12.00, and 16.00 kPa is shown in Table 1. Stiffness was highest in the posterior region and lowest in the anterior region. Differences among the four regions became larger as pressure increased. Fig. 8(c) shows mean stiffness and significance differences at a transmural pressure of 12.00 kPa. There was significant difference in the mean stiffness among the four regions above a transmural pressure of 8.00 kPa, such as between the anterior and posterior regions and the posterior and right lateral regions. The mean pressure–strain elastic modulus, however, did not differ significantly among the four regions (Fig. 8(d)).

Please cite this article as: Kim, J., Baek, S., Circumferential variations of mechanical behavior of the porcine thoracic aorta during the inflation test. Journal of Biomechanics (2011), doi:10.1016/j.jbiomech.2011.04.022

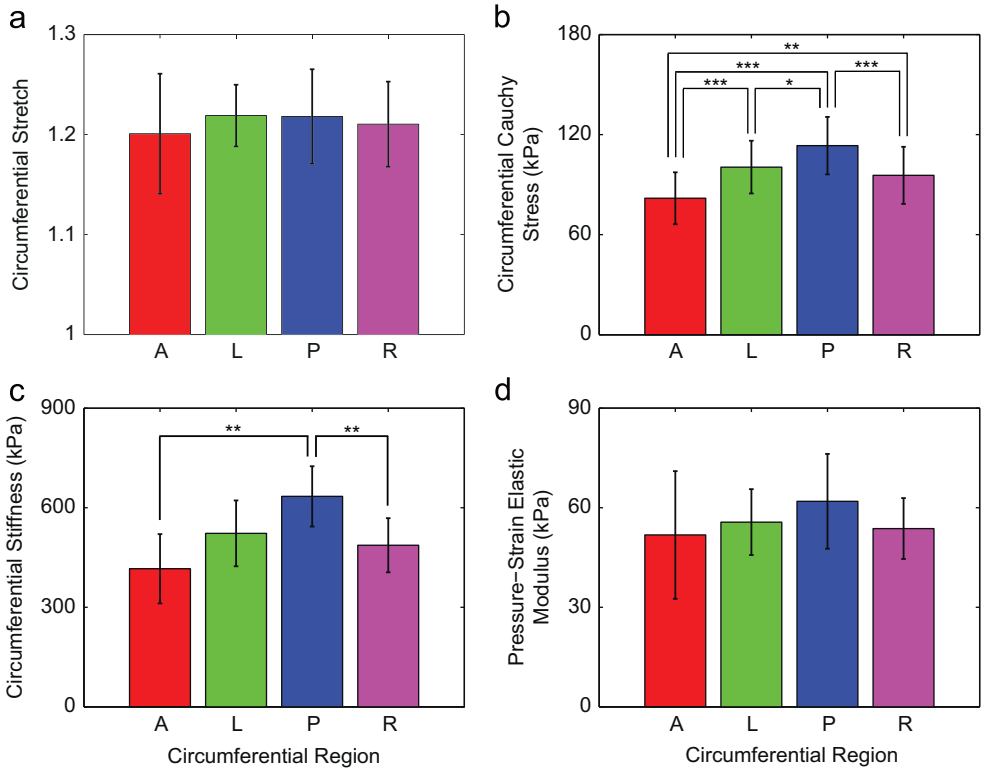


**Fig. 8.** Mean and standard deviation of circumferential stretch (a), circumferential Cauchy stress (b), circumferential stiffness (c), and pressure–strain elastic modulus (d), at a transmural pressure of 12.00 kPa and $\Lambda_Z = 1.35$. Asterisks represent significant differences ($^{*}: p < 0.05, ^{**}: p < 0.01, ^{***}: p < 0.001$).

**Table 1**
The mean stiffness and standard deviation of the circumferential stiffness at the transmural pressures of 8.00, 12.00, and 16.00 kPa for each circumferential region (unit: kPa).

| Region | 8.00 kPa | 12.00 kPa | 16.00 kPa |
|---|---|---|---|
| Anterior | $310 \pm 47$ | $416 \pm 104$ | $671 \pm 185$ |
| Left lateral | $359 \pm 33$ | $523 \pm 99$ | $1065 \pm 255$ |
| Posterior | $419 \pm 58$ | $634 \pm 91$ | $1246 \pm 136$ |
| Right lateral | $347 \pm 50$ | $489 \pm 82$ | $964 \pm 117$ |

## 5. Discussion

In the present study, the circumferential variation in stiffness of the porcine descending thoracic aorta was experimentally investigated. In order to characterize the local mechanical properties of the aorta, we developed an *ex vivo* extension-inflation experimental apparatus with a stereo vision system, which allowed us to measure the 3D deformation of a blood vessel, and a stress–strain analysis method using the 3D experimental data. Our major finding was that the posterior region of the porcine thoracic aorta was significantly stiffer than the anterior. However, the posterior region was significantly thinner than the anterior, so that the structural stiffness represented by the pressure–strain elastic modulus remained non-significant. This finding suggests that the circumferential distention of the proximal descending thoracic aorta may be uniform *in vivo* even with the significant circumferential variations in stiffness of the vascular tissue. However, the validation of this suggestion requires a better understanding of the effect of surrounding tissues and the spine on biomechanics of aortic wall *in vivo*.

All circumferential regions of the thoracic aorta exhibited similar nonlinear behavior (Fig. 7(a)). The circumferential stress increased linearly up to a transition point beyond which the stress increased rapidly in response to increased stretch. This nonlinear trend of the circumferential stress of the thoracic aorta is consistent with other studies on the human (Spina et al., 1983), the canine (Zhou and Fung, 1997), and the ovine (Wells et al., 1999) thoracic aortas. The stress–stretch response in our study remained linear up to a relatively higher pressure than in other porcine arteries, such as porcine basilar and coronary arteries (Hu et al., 2007; Pandit et al., 2005; Wang et al., 2006).

The transition from linear to nonlinear behavior of the aorta occurred at 10.93–14.53 kPa (82–109 mmHg), which falls within the *in vivo* pressure range from 10.13 to 15.20 kPa (76–114 mmHg) when the radial compression of the aorta by the surrounding tissue is assumed to be around 5% of internal pressure (Zhang et al., 2005). Other studies have also suggested that the transition corresponded to normal physiological conditions (Danpinid et al., 2010; Shadwick, 1999).

Many studies have reported that elastin fibers are primarily responsible for the linear behavior of an artery in the low pressure range (Gundiah et al., 2007; Shadwick, 1999; Stergiopulos et al., 2001). The influence of elastin on the mechanical properties of aortic tissue has been investigated (Gundiah et al., 2007; Lillie and Gosline, 2007; Zou and Zhang, 2009). The stiffness of the aortic wall may be affected by the amount of elastin, the orientation of elastin fibers, and the density of cross-linking. On the other hand, collagen is recruited in the higher pressure range and contributes to the nonlinear behavior of arterial tissue (Groenink et al., 1999; Shadwick, 1999). The orientation of collagen fibers and the amount of cross-linking influence the mechanical behavior of vascular tissue (Haskett et al., 2010; Holzapfel et al., 2002). Therefore, histological and microstructural features may be correlated with the circumferential heterogeneity of the mechanical properties of the aorta.

Limitations of our experiment include possible measurement errors caused by the rotation of the aorta when measuring the strain at the four circumferential regions of the aorta. The accuracy of the experiments may be enhanced by using multiple

Please cite this article as: Kim, J., Baek, S., Circumferential variations of mechanical behavior of the porcine thoracic aorta during the inflation test. Journal of Biomechanics (2011), doi:10.1016/j.jbiomech.2011.04.022

cameras simultaneously around the specimen or using a concave conical mirror (Genovese, 2009). Another shortcoming of this study is that we used only the circumferential stress and stretch for estimating the stiffness. Hence, there is a need for an enhanced method for accurately analyzing the regional biaxial mechanical behavior of the vessel wall.

Finally, we suggest that the experimental method and analysis presented in this paper can be used in the study of vascular adaptation during the progression of vascular diseases, which will eventually increase our understanding of the role of biomechanics on vascular diseases or vice versa.

## Conflict of interest

We do not have a conflict of interest with anyone or organization.

## Appendix A. Supplementary data

Supplementary data associated with this article can be found in the online version at doi:10.1016/j.jbiomech.2011.04.022.

## References

Avril, S., Badel, P., Duprey, A., 2010. Anisotropic and hyperelastic identification of *in vitro* human arteries from full-field optical measurements. Journal of Biomechanics 43, 2978–2985.

Blondel, W.C.P.M., Didelon, J., Maurice, G., Carteaux, J.P., Wang, X., Stoltz, J.F., 2001. Investigation of 3-D mechanical properties of blood vessels using a new *in vitro* tests system: results on sheep common carotid arteries. IEEE Transactions on Biomedical Engineering 48, 442–451.

Carew, T.E., Vaishnav, R.N., Patel, D.J., 1968. Compressibility of the arterial wall. Circulation Research 23, 61–68.

Danpinid, A., Luo, J., Vappou, J., Terdtoon, P., Konofagou, E.E., 2010. *In vivo* characterization of the aortic wall stress–strain relationship. Ultrasonics 50, 654–665.

Draney, M.T., Arko, F.R., Alley, M.T., Markl, M., Herfkens, R.J., Pelc, N.J., Zarins, C.K., Taylor, C.A., 2004. Quantification of vessel wall motion and cyclic strain using cine phase contrast MRI: *in vivo* validation in the porcine aorta. Magnetic Resonance in Medicine 52, 286–295.

Draney, M.T., Herfkens, R.J., Hughes, T.J.R., Pelc, N.J., Wedding, K.L., Zarins, C.K., Taylor, C.A., 2002. Quantification of vessel wall cyclic strain using cine phase contrast magnetic resonance imaging. Annals of Biomedical Engineering 30, 1033–1045.

Everett, W.N., Shih, P., Humphrey, J.D., 2005. A bi-plane video-based system for studying the mechanics of arterial bifurcations. Experimental Mechanics 45, 377–382.

Feigl, E.O., Peterson, L.H., Jones, A.W., 1963. Mechanical and chemical properties of arteries in experimental hypertension. Journal of Clinical Investigation 42, 1640–1647.

Genovese, K., 2009. A video-optical system for time-resolved whole-body measurement on vascular segments. Optics and Lasers in Engineering 47, 995–1008.

Groenink, M., Langerak, S.E., Vanbavel, E., van der Wall, E.E., Mulder, B.J.M., van der Wal, A.C., Spaan, J.A.E., 1999. The influence of aging and aortic stiffness on permanent dilation and breaking stress of the thoracic descending aorta. Cardiovascular Research 43, 471–480.

Gundiah, N., Ratcliffe, M.B., Pruitt, L.A., 2007. Determination of strain energy function for arterial elastin: experiments using histology and mechanical tests. Journal of Biomechanics 40, 586–594.

Guo, X., Kassab, G.S., 2004. Distribution of stress and strain along the porcine aorta and coronary arterial tree. American Journal of Physiology - Heart and Circulatory Physiology 286, H2361–H2368.

Han, H.C., Fung, Y.C., 1995. Longitudinal strain of canine and porcine aortas. Journal of Biomechanics 28, 637–641.

Haskett, D., Johnson, G., Zhou, A., Utzinger, U., Vande Geest, J., 2010. Microstructural and biomechanical alterations of the human aorta as a function of age and location. Biomechanics and Modeling in Mechanobiology 9, 725–736.

Holzapfel, G.A., Gasser, T.C., Stadler, M., 2002. A structural model for the viscoelastic behavior of arterial walls: continuum formulation and finite element analysis. European Journal of Mechanics-A/Solids 21, 441–463.

Hsu, F.P.K., Liu, A.M.C., Downs, J., Rigamonti, D., Humphrey, J.D., 1995. A triplane video-based experimental system for studying axisymmetrically inflated biomembranes. IEEE Transactions on Biomedical Engineering 42, 442–450.

Hu, J.J., Fossum, T.W., Miller, M.W., Xu, H., Liu, J.C., Humphrey, J.D., 2007. Biomechanics of the porcine basilar artery in hypertension. Annals of Biomedical Engineering 35, 19–29.

Huang, Y., Guo, X., Kassab, G.S., 2006. Axial nonuniformity of geometric and mechanical properties of mouse aorta is increased during postnatal growth. American Journal of Physiology- Heart and Circulatory Physiology 290, H657–H664.

Humphrey, J.D., Kang, T., Sakarda, P., Anjanappa, M., 1993. Computer-aided vascular experimentation: a new electromechanical test system. Annals of Biomedical Engineering 21, 33–43.

Lally, C., Reid, A.J., Prendergast, P.J., 2004. Elastic behavior of porcine coronary artery tissue under uniaxial and equibiaxial tension. Annals of Biomedical Engineering 32, 1355–1364.

Langewouters, G.J., Wesseling, K.H., Goedhard, W.J.A., 1984. The static elastic properties of 45 human thoracic and 20 abdominal aortas *in vitro*and the parameters of a new model. Journal of Biomechanics 17, 425–435.

Lillie, M.A., Gosline, J.M., 2007. Mechanical properties of elastin along the thoracic aorta in the pig. Journal of Biomechanics 40, 2214–2221.

Okamoto, R.J., Wagenseil, J.E., DeLong, W.R., Peterson, S.J., Kouchoukos, N.T., Sundt III, T.M., 2002. Mechanical properties of dilated human ascending aorta. Annals of Biomedical Engineering 30, 624–635.

Pandit, A., Lu, X., Wang, C., Kassab, G.S., 2005. Biaxial elastic material properties of porcine coronary media and adventitia. American Journal of Physiology - Heart and Circulatory Physiology 288, H2581–H2587.

Peterson, L.H., Jensen, R.E., Parnell, J., 1960. Mechanical properties of arteries *in vivo*. Circulation Research 8, 622–639.

van Prehn, J., Vincken, K.L., Sprinkhuizen, S.M., Viergever, M.A., van Keulen, J.W., van Herwaarden, J.A., Moll, F.L., Bartels, L.W., 2009. Aortic pulsatile distention in young healthy volunteers is asymmetric: analysis with ECG-gated MRI. European Journal of Vascular and Endovascular Surgery 37, 168–174.

Saravanan, U., Baek, S., Rajagopal, K.R., Humphrey, J.D., 2006. On the deformation of the circumflex coronary artery during inflation tests at constant length. Experimental Mechanics 46, 647–656.

Schulze-Bauer, C.A.J., Morth, C., Holzapfel, G.A., 2003. Passive biaxial mechanical response of aged human iliac arteries. ASME Journal of Biomechanical Engineering 125, 395–406.

Schulze-Bauer, C.A.J., Regitnig, P., Holzapfel, G.A., 2002. Mechanics of the human femoral adventitia including the high-pressure response. American Journal of Physiology - Heart and Circulatory Physiology 282, H2427–H2440.

Shadwick, R.E., 1999. Mechanical design in arteries. Journal of Experimental Biology 202, 3305–3313.

Shapiro, L.G., Stockman, G.C., 2001. Computer Vision. Prentice Hall, New Jersey.

Sokolis, D.P., 2007. Passive mechanical properties and structure of the aorta: segmental analysis. Acta Physiologica 190, 277–289.

Spina, M., Garbisa, S., Hinnie, J., Hunter, J.C., Serafini-Fracassini, A., 1983. Age-related changes in composition and mechanical properties of the tunica media of the upper thoracic human aorta. Arteriosclerosis, Thrombosis, and Vascular Biology 3, 64–76.

Stergiopulos, N., Vulliemoz, S., Rachev, A., Meister, J.J., Greenwald, S.E., 2001. Assessing the homogeneity of the elastic properties and composition of the pig aortic media. Journal of Vascular Research 38, 237–246.

Struik, D.J., 1988. Lectures on Classical Differential Geometry, second ed. Dover Publications, Inc., New York.

Thubrikar, M.J., Roskelley, S., Eppink, R., 1990. Study of stress concentration in the walls of the bovine coronary arterial branch. Journal of Biomechanics 23, 15–17.

Tremblay, D., Cartier, R., Mongrain, R., Leask, R.L., 2010. Regional dependency of the vascular smooth muscle cell contribution to the mechanical properties of the pig ascending aortic tissue. Journal of Biomechanics 43, 2448–2451.

Valdez-Jasso, D., Haider, M.A., Banks, H.T., Bia Santana, D., German, Y.Z., Armentano, R.L., Olufsen, M.S., 2009. Analysis of viscoelastic wall properties in ovine arteries. IEEE Transaction on Biomedical Engineering 56, 210–219.

Vande Geest, J.P., Sacks, M.S., Vorp, D.A., 2006. The effects of aneurysm on the biaxial mechanical behavior of human abdominal aorta. Journal of Biomechanics 39, 1324–1334.

Wang, C., Garcia, M., Lu, X., Lanir, Y., Kassab, G.S., 2006. Three-dimensional mechanical properties of porcine coronary arteries: a validated two-layer model. American Journal of Physiology - Heart and Circulatory Physiology 291, H1200–H1209.

Wells, S.M., Langille, B.L., Lee, J.M., Adamson, S.L., 1999. Determinants of mechanical properties in the developing ovine thoracic aorta. American Journal of Physiology - Heart and Circulatory Physiology 277, H1385–H1391.

Zhang, D., Eggleton, C.D., Arola, D.D., 2002. Evaluating the mechanical behavior of arterial tissue using digital image correlation. Experimental Mechanics 42, 409–416.

Zhang, W., Herrera, C., Atluri, S.N., Kassab, G.S., 2005. The effect of longitudinal pre-stretch and radial constraint on the stress distribution in the vessel wall: a new hypothesis. Mechanics and Chemistry of Biosystems 2, 41–52.

Zhou, J., Fung, Y.C., 1997. The degree of nonlinearity and anisotropy of blood vessel elasticity. Proceedings of the National Academy of Sciences 94, 14255–14260.

Zou, Y., Zhang, Y., 2009. An experimental and theoretical study on the anisotropy of elastin network. Annals of Biomedical Engineering 37, 1572–1583.

Please cite this article as: Kim, J., Baek, S., Circumferential variations of mechanical behavior of the porcine thoracic aorta during the inflation test. Journal of Biomechanics (2011), doi:10.1016/j.jbiomech.2011.04.022